

ZONED TOURMALINE ASSOCIATED WITH CASSITERITE: IMPLICATIONS FOR FLUID EVOLUTION AND TIN MINERALIZATION IN THE SAN RAFAEL Sn-Cu DEPOSIT, SOUTHEASTERN PERU

MICHAEL S.J. MLYNARCZYK[§] AND ANTHONY E. WILLIAMS-JONES

Department of Earth & Planetary Sciences, McGill University, 3450 University Street, Montreal, Quebec H3A 2A7, Canada

Abstract

The composition of tourmaline in the San Rafael Sn-Cu lode, in southeastern Peru, provides an important record of the early evolution of the hydrothermal system that produced the world's richest tin deposit. Many forms, colors and compositions of tourmaline, ranging from dravite to schorl, are present in the deposit, but the late tourmaline that accompanied deposition of early cassiterite has an unusual dark green color, and exhibits a strong trend of enrichment in iron. Appearance of this tourmaline in the paragenesis coincided with a marked change in the vein style, reflecting an opening of the vein system, and a dramatic change in the mineralogy of vein and alteration assemblages, evident from the precipitation of other iron-rich minerals (Fe-rich chlorite and cassiterite). This abrupt change in the plumbing of the hydrothermal system was associated with the introduction of dilute, relatively oxidizing, externally derived waters of meteoric origin that mixed with hot magmatic brines carrying high concentrations of dissolved tin and iron. The resulting sudden cooling, dilution, and oxidation of the ore fluids created the conditions required for massive precipitation of cassiterite and formation of a very large, high-grade ore deposit.

Keywords: tourmaline, schorl, cassiterite, tin lode, iron, crystal zonation, San Rafael, Peru.

SOMMAIRE

La composition de la tourmaline dans le système de veines à Sn-Cu de San Rafael, dans le sud-est du Pérou, témoigne de façon directe les stades précoces dans l'évolution du système hydrothermal responsable du gisement d'étain le plus riche du monde. Plusieurs morphologies, couleurs et compositions de tourmaline, variant de dravite à schorl, sont présentes dans ce gisement, mais la tourmaline tardive qui a accompagné la précipitation de la cassitérite précoce possède une couleur verte inhabituelle, et fait preuve d'un fort enrichissement en fer. L'apparition de cette génération de tourmaline dans la paragenèse a coïncidé avec un changement abrupt du type de veine, réflexion d'une ouverture du système, et d'un changement dramatique dans la minéralogie des veines et des assemblages d'altération, en particulier la précipitation d'autres minéraux riches en fer comme la chlorite et la cassitérite ferrifères. Ce changement du système de circulation hydrothermale fut associé avec l'introduction d'eau diluée, relativement oxydante et d'origine météorique, dérivée d'une source externe, qui s'est mélangée avec des saumures chaudes issues du magma, porteuses d'étain et de fer. Le refroidissement soudain, la dilution, et l'oxydation de la phase fluide minéralisante ont créé les conditions requises pour une précipitation massive de cassitérite et la formation d'un gisement énorme à teneur élevée.

(Traduit par la Rédaction)

Mots-clés: tourmaline, schorl, cassitérite, veines riches en étain, fer, zonation des cristaux, San Rafael, Pérou.

INTRODUCTION

Tourmaline is a common gangue mineral in a variety of hydrothermal ore deposits, including granite-related tin lodes, Cu-Mo and Au porphyries, shear-zone-hosted gold veins and sediment-hosted massive-sulfide deposits (Slack 1996). Because it is stable over a wide range of temperature and pressure, and can incorporate many trace elements into its structure (Henry & Dutrow 1996), tourmaline generally preserves a very

good record of the composition of the fluid from which it crystallized. Consequently, the composition of tourmaline can be used to interpret the origin and evolution of the ore fluids, thereby providing a potentially valuable tool for mineral exploration (Taylor & Slack 1984, Slack & Coad 1989, Cavaretta & Puxeddu 1990, London & Manning 1995, Lynch & Ortega 1997, Jiang *et al.* 1998, Pirajno & Smithies 1992, Griffin *et al.* 1996, Williamson *et al.* 2000).

[§] E-mail address: michael@eps.mcgill.ca

Here, we describe several generations of tourmaline from the San Rafael deposit, a world-class hydrothermal tin lode in the Eastern Cordillera of the Peruvian Central Andes, where tourmaline is the principal mineral in rocks altered by an early, barren stage of hydrothermal activity that preceded main-stage tin mineralization. Tourmaline is also present in early cassiterite-bearing veins. As the composition of tourmaline is very sensitive to physicochemical changes in the hydrothermal environment, we have used the composition of the San Rafael tourmaline to reconstruct the evolution of fluids in the deposit and to identify the physicochemical triggers that led to the formation of the rich tin ores.

GEOLOGICAL SETTING

San Rafael lies in the high mountains of the Eastern Cordillera of southeastern Peru, and is a world-class Sn–Cu deposit. It has an average ore-grade of ~5 wt.% Sn, hosts a total resource of ~1 million tonnes of tin metal (production + reserves), and accounts for nearly a fifth of the world's current hard-rock production of tin (Minsur S.A., unpubl. data, 2000, Carlin 2005). The deposit consists of a series of subparallel, northwest-trending and northeast-dipping veins, up to 3 km in length, that are centered on a shallow-level Late Oligocene granitic pluton (Fig. 1). This intrusion, which has an outcrop area of less than 15 km², is largely buried, and only a contact aureole of hornfelsed lower Paleozoic slate indicates its considerable subsurface extent. The main rock-types in the pluton are coarse- to medium-grained biotite- and cordierite-bearing granite

and granodiorite, which typically contain abundant K-feldspar megacrysts. The intrusive suite is peraluminous, belongs to the S-type category of granitic rocks of Chappell & White (1974) and the CPG category of granitic rocks of Barbarin (1999).

The bulk of the ore is contained in a single, complex vein-breccia system, the San Rafael lode, which can be traced down-dip for more than 1,200 meters, and is hosted mainly by granitic rocks. The lode comprises a narrow chalcopyrite-rich upper zone that contains disseminated acicular cassiterite, and a lower zone of 10- to 50-m-wide fault jogs that contain the bulk of the tin ore in cassiterite – quartz – chlorite veins and breccias. Both ore types are associated with strong chloritic alteration, which forms a 10- to 15-meter-wide envelope around the vein–breccia system.

As indicated by cross-cutting relations and vein paragenesis, the sequence of hydrothermal events started with a barren stage that formed abundant tourmaline – quartz ± arsenopyrite veins and tourmaline–quartz microbreccias, with associated intense white mica and tourmaline alteration of the wallrocks. This early stage was followed by strong, laterally extensive formation of chlorite, which overprinted all earlier alteration-induced minerals (except tourmaline), and by the large-scale precipitation of cassiterite (wood-tin, banded to botryoidal cassiterite, and “needle tin” varieties). During a later stage of this protracted mineralizing event, sulfide ores (mostly chalcopyrite) were deposited. Hydrothermal activity culminated in the formation of abundant barren veins of quartz, which cut the earlier veins and alteration envelopes.

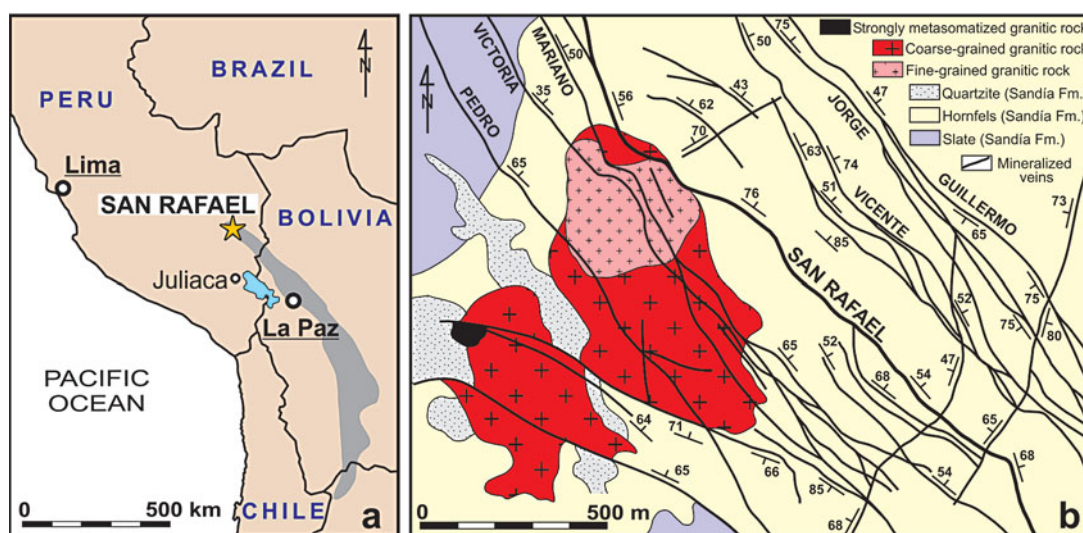


FIG. 1. a) Location of the San Rafael deposit (star) with respect to the Central Andean Sn–W–(Ag) metallogenic province (grey outline, modified after Lehmann 1979). b) Geological map of the southwestern part of the San Rafael district (modified after Arenas 1980).

In Figure 2, we summarize the deposit paragenesis and the results of a preliminary fluid-inclusion study. A more detailed description of the ores and alteration is given in Mlynarczyk *et al.* (2003, 2006a), and data on fluid inclusions and stable isotope geochemistry are presented in Mlynarczyk *et al.* (2006b).

TOURMALINE PARAGENESIS

Magmatic and postmagmatic tourmaline

Magmatic tourmaline is restricted to occurrences in minor late-stage plugs and dykes of tourmaline leucogranite, which crop out along the southwestern and northeastern margins of the pluton. This tourmaline forms small (40–400 μm), yellow (in thin section), euhedral to subhedral prismatic crystals that are disseminated throughout the rock (~5 vol.%, Fig. 3a). The tourmaline leucogranite represents the latest and most evolved phase of the pluton, but its genetic relationship to the hydrothermal tourmaline still needs to be evaluated.

Early postmagmatic tourmaline is not very abundant, but occurs throughout the main granite–granodiorite suite. It can be distinguished from magmatic tourmaline by its blue color (in thin section) and common replacement of cordierite phenocrysts. Since this postmagmatic tourmaline is not associated with tourmaline veinlets and occurs in rocks that otherwise appear unaltered, it is interpreted to have formed very soon after crystallization of the pluton. It is similar to blue dravite that

replaced cordierite in Li-poor granitic pegmatites of the Moldanubicum region, Czech Republic, and is attributed to reaction of cordierite with pegmatite-derived, acidic, B-rich fluids at an early stage of subsolidus crystallization (Novák 1998).

Early hydrothermal tourmaline

The bulk of the tourmaline in the San Rafael deposit is associated with the early, barren stage of the hydrothermal system. Volumetrically, the largest amounts of tourmaline are hosted by dyke-like tourmaline–quartz microbreccias of hydrothermal origin that follow the tin lode along strike for hundreds of meters and, locally, exceed 5 meters in width. In these rocks, tourmaline is yellow in thin section, and occurs both in the clasts and the matrix of the breccia, which typically is very fine-grained (Fig. 3b). The clasts are composed of fragments of strongly tourmalinized wallrock and vein tourmaline, as well as fragments of tourmaline–quartz microbreccia, indicating a history of repeated brittle deformation.

Tourmaline (mostly yellow in thin section) is also very abundant in the early veins and their alteration envelopes. Tourmaline–quartz veins are generally narrow (<3 cm), but ubiquitous throughout the pluton, and commonly contain arsenopyrite that is either disseminated in vein selvages or fills open spaces between tourmaline crystals (Fig. 4a). These barren veins form conjugate sets, one striking ~295° and dipping SW, and the other striking ~330° and dipping NE. The latter set was subsequently re-opened and

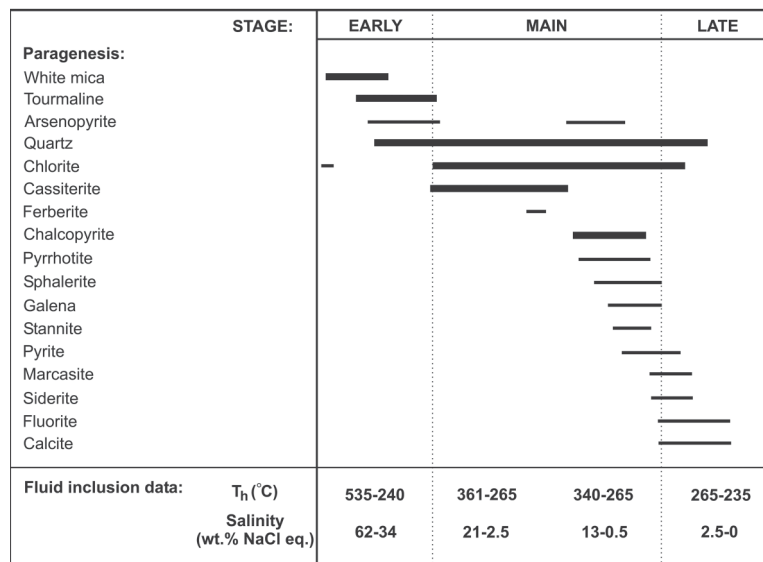


FIG. 2. Simplified paragenesis for the San Rafael deposit and summary of preliminary fluid-inclusion data. The thickness of the horizontal lines indicates the abundance of the mineral species.

mineralized during the main tin-ore event. Most tourmaline-quartz veins form swarms and, locally, denser stockworks characterized by multiple generations of veins. These veins are commonly rimmed by an envelope of strong alteration to tourmaline, which grades outward into a zone (≤ 25 cm) of intense alteration to white mica.

Where replacement by tourmaline was particularly intense, tourmaline replaced all ferromagnesian minerals and feldspars, in a sequence from cordierite and calcium-rich plagioclase ($An_{>25}$), through biotite and white mica, to sodic plagioclase ($An_{<25}$) and K-feldspar. Quartz is the only mineral preserved from the original granitic assemblage. In addition, outlines of the replaced phenocrysts (biotite, cordierite and the feldspars) are also commonly preserved (Fig. 3c). Whereas the replacement of biotite and feldspar produced tourmaline of yellow color in thin section, replacement of cordierite produced pale blue tourmaline.

Vein tourmaline (*i.e.*, tourmaline that precipitated from the hydrothermal fluids, as opposed to that formed by replacement of pre-existing minerals), generally has a more variable appearance than alteration-induced tourmaline. Moreover, several generations that can be distinguished optically may be present within the same sample. In hand specimen, vein tourmaline is commonly light to dark brown in color, but locally it exhibits orange, creamy, or beige tints. In thin section (plane-polarized light), it is typically yellow, colorless or blue, and generally strongly pleochroic with $\omega \gg \epsilon$ (Figs. 3d, e). The habit ranges from short-prismatic to acicular (in vugs) but, unlike the magmatic tourmaline, which is optically homogeneous, tourmaline crystals in veins commonly show marked zoning in color and composition (Figs. 3f, 4b). Locally, these crystals also display very fine growth-lamellae, a feature that has been observed in hydrothermal tourmaline elsewhere (Slack & Coad 1989, Cavaretta & Puxeddu 1990, London & Manning 1995). On the basis of cross-cutting relations among tourmaline veinlets, we conclude that yellow tourmaline (plane-polarized light) was followed paragenetically by colorless or orange tourmaline and, in turn, by dark blue, pale blue, or pale green tourmaline (Figs. 5, 6a, 6b).

Ore-stage tourmaline

The majority of tourmaline-quartz veins were sealed prior to ore deposition, but a few remained open, and contain a second generation of tourmaline, which coprecipitated with abundant cassiterite and chlorite. In contrast to the former veins, these Sn-rich veins display evidence of clear open-space filling, and are surrounded by halos of intensely chloritized wallrocks. In cross-section, they typically comprise an outer zone of massive, monomineralic tourmaline several cm thick; the tourmaline is colorless or orange in thin section (Fig. 5). This zone is succeeded inward by a zone of

green tourmaline that rimmed, replaced, and locally cut the earlier (colorless or orange) tourmaline (Figs. 5, 6c, 6d). The next zone, which is narrow and irregular, is composed of very fine, radial aggregates of needle-like cassiterite (Fig. 6e). It is succeeded, in turn, by a relatively porous zone of coarse, euhedral crystals of cassiterite intimately intergrown with bundles of acicular khaki-green to dark-green tourmaline (Fig. 6f) and minor chlorite. Finally, the vein core comprises coarse, monomineralic arsenopyrite, which is commonly euhedral, owing to its open-space deposition (Fig. 5).

The massive deposition of cassiterite that followed the formation of the latter multistage veins was associated with strong, deposit-wide chloritization, which largely obliterated earlier white mica alteration (Mlynarczyk *et al.* 2003, 2006a). Pre-existing tourmaline, hosted by the breccias, the early veins, and their alteration envelopes, however, was largely unaffected. Thus, even in wallrock, which was so strongly chloritized that it now consists only of chlorite and quartz, tourmaline crystals commonly retain their original color-zoning. Nonetheless, at high magnification, most crystals of tourmaline in rocks affected by chloritic alteration are seen to have a thin overgrowth of a late, greenish variety of tourmaline (Figs. 6g, 6h). These overgrowths are optically continuous with the host crystal and form a narrow (5–100 μm) rim or jagged terminations. Owing to their pale green to blue-green color, they would be easily overlooked were it not for their interference colors, which are much higher than those of the surrounding chlorite. In addition to the near-ubiquitous green overgrowths, an irregular rim of bluish grey color also occurs on some early crystals of tourmaline.

Ore-stage tourmaline that coprecipitated with abundant chlorite locally formed new crystals, as shown by a sample containing a complex intergrowth of very fine needles of tourmaline and chlorite. This is consistent with the fact that the vast majority of vein- and breccia-hosted samples of tourmaline, even those collected away from zones of chloritization, are cut by fine veinlets containing needles of late, greenish or bluish tourmaline (Fig. 6b), in addition to quartz and, locally, chlorite. In summary, there is ample evidence that tourmaline continued to form after the onset of ore deposition, albeit in volumetrically minor amounts and with a marked difference in color, relative to the earlier assemblages.

ANALYTICAL METHODS

Forty-six polished thin sections of tourmaline-bearing samples were prepared. Electron-microprobe analyses (636 analyses on 151 individual tourmaline zones or grains) were carried out at the Department of Earth and Planetary Sciences of McGill University, using a JEOL JXA-8900L instrument, and at the Faculty of Geology of the University of Warsaw in

Poland, using a CAMECA SX–100 instrument. Detailed X-ray maps of Mg, Fe, Na, and Sn were obtained for a late, complexly zoned crystal of tourmaline. Analytical conditions were the same for both electron microprobes: accelerating voltage 15 kV, beam current 20 nA, and spot size 5 μm . The detection limits for Sn and W were 200 and 2000 ppm, respectively, but owing to the necessity of extending the counting time, only selected samples were analyzed for these two elements. For standards, we used natural and synthetic materials: albite (Na), diopside (Si, Ca, Mg), orthoclase (K, Al), hematite (Fe), spessartine (Mn), TiO_2 (Ti), chromite (Cr), fluorite (F), vanadinite (Cl) and, for a subset of analyses, cassiterite (Sn) and scheelite (W). Cation proportions were calculated using the $T + Z + Y = 15$ scheme (Henry & Dutrow 1996), and we assumed all Fe to be ferrous (Table 1).

As ferrous–ferric iron recalculations based on electron-microprobe data rely largely on assumptions that cannot be easily verified, and the determination of Fe^{3+} and Fe^{2+} in tourmaline by Mössbauer spectroscopy requires pure, homogeneous samples in amounts larger than typically available in this study, wet-chemical methods were used to estimate the proportions of ferrous and ferric iron. However, determination of the ratio $\text{Fe}^{2+}/\text{Fe}^{3+}$ in tourmaline by wet-chemical methods is problematic, owing to the refractory behavior of tourmaline in cold acids and the oxidation of much of its ferrous iron during dissolution in hot acids (Ingamells 1960, Weiss 1969, Bouvier *et al.* 1972, Povondra & Čech 1976, Povondra & Ulrych 1976). The analytical results reported here are, therefore, semiquantitative at best in that they only provide a minimum estimate of the ferrous iron content of tourmaline. In total, fifteen separates of the most homogeneous tourmaline available were carefully hand-picked under a binocular microscope and finely ground. The total iron content was established by atomic absorption with fusion preparation at the Department of Earth and Planetary Sciences of McGill University. Ferrous iron was determined by dissolving the samples in cold hydrofluoric acid for an extended period of time (more than three weeks), while constantly stirring, and subsequent ammonium metavanadate titration. Ferric iron was calculated from the difference between total iron and ferrous iron. In order to assess the quality of the data obtained, five tourmaline standards (112566 schorl, 108796 dravite, 98144 elbaite, STRGR–2 schorl; Dyar *et al.* 1998, 2001, and type-locality buergerite) with the $\text{Fe}^{3+}/\text{Fe}^{2+}$ ratio determined by independent methods (Mössbauer and XANES spectroscopies) also were analyzed.

COMPOSITION OF THE TOURMALINE

Major elements

Tourmaline is a complex borosilicate mineral with the general structural formula: $\text{XY}_3\text{Z}_6[\text{T}_6\text{O}_{18}][\text{BO}_3]_3\text{V}_3\text{W}$,

where $X = \text{Ca, Na, K, } \square$ (vacancy); $Y = \text{Li, Mg, Fe}^{2+}, \text{Mn}^{2+}, \text{Al, Cr}^{3+}, \text{V}^{3+}, \text{Fe}^{3+}, (\text{Ti}^{4+})$; $Z = \text{Mg, Al, Fe}^{3+}, \text{V}^{3+}, \text{Cr}^{3+}, (\text{Fe}^{2+})$; $T = \text{Si, Al, B}$; $B = \text{B, } \square$; $V = \text{OH}^-, \text{O}^{2-}$; $W = \text{OH}^-, \text{F}^-, \text{O}^{2-}$. The species in parentheses have not yet been proven to occur at these sites. The V and W sites are also referred to as the $[\text{O}(3)]$ site and $[\text{O}(1)]$ site, respectively (Henry & Dutrow 1996, Hawthorne & Henry 1999). Substitutions at the X, Y, Z, V , and W sites are common, and yield a wide range of tourmaline end-members, 14 of which are IMA-approved [see Hawthorne & Henry (1999) for review]. End-members that do not correspond to established minerals are shown below in quotation marks.

Representative results of electron-microprobe analyses and corresponding sample descriptions of tourmaline from San Rafael are listed in Table 1, and Figure 7 presents plots of Al–Fe–Mg and $\text{Ca–X}\square\text{–}(\text{Na} + \text{K})$ variation for two sets of averaged compositions of tourmaline. Set A shows the evolution of tourmaline compositions in a single tourmaline – cassiterite – chlorite – arsenopyrite vein of the type described above (Fig. 5), in which four successive generations of tourmaline (colorless, orange, green, and dark green in plane-polarized light) are distinguished. The compositions of all other tourmaline crystals from the deposit constitute set B, and are grouped into the following categories: magmatic, microbreccia-hosted, very early alteration, early alteration (barren stage), vein tourmaline, and late (greenish) overgrowths and rims on earlier tourmaline.

The composition of most samples corresponds to that of the dravite–schorl solid-solution series, extending toward the alkali-free (“Mg-foitite” and foitite) and oxy-tourmaline (“oxy-dravite” and “oxy-schorl”) end-members (Fig. 7). Overall, the San Rafael tourmaline is Ca- and K-poor, with $\text{Na}/(\text{Na} + \text{Ca})$ typically between 0.70 and 0.99 (average: 0.88) and $\text{K} < 0.01$ *apfu* (atoms per formula unit). Following the X -site-based classification of Hawthorne & Henry (1999), it belongs to the alkali tourmaline group, with the exception of a few samples that have a large proportion of vacancies at the X site (Fig. 7). If the Y site is considered, the principal compositional trend is an evolution to systematically higher concentrations of total Fe, observed both in single-vein set A and the deposit-scale set B. Thus, the $\text{Fe}/(\text{Fe} + \text{Mg})$ value increases from as low as 0.02 (nearly pure dravite) to 0.87 (schorl), averaging ~ 0.44 ; whereas the bulk of the early, barren-stage tourmaline is Fe-bearing dravite, the late tourmaline is Mg-bearing schorl. The magmatic tourmaline is also Fe-rich, with a $\text{Fe}/(\text{Fe} + \text{Mg})$ value of ~ 0.73 . A large overlap exists between the compositions of alteration, microbreccia-hosted, and vein tourmaline. The Li content was not determined, but is considered to be negligible, as bulk-rock analyses of strongly tourmalinized rocks (up to 45 vol.% tourmaline) contain less than 100 ppm Li (Mlynarczyk *et al.* 2006a). Appreciable Li would be associated with an increased Al content (toward the

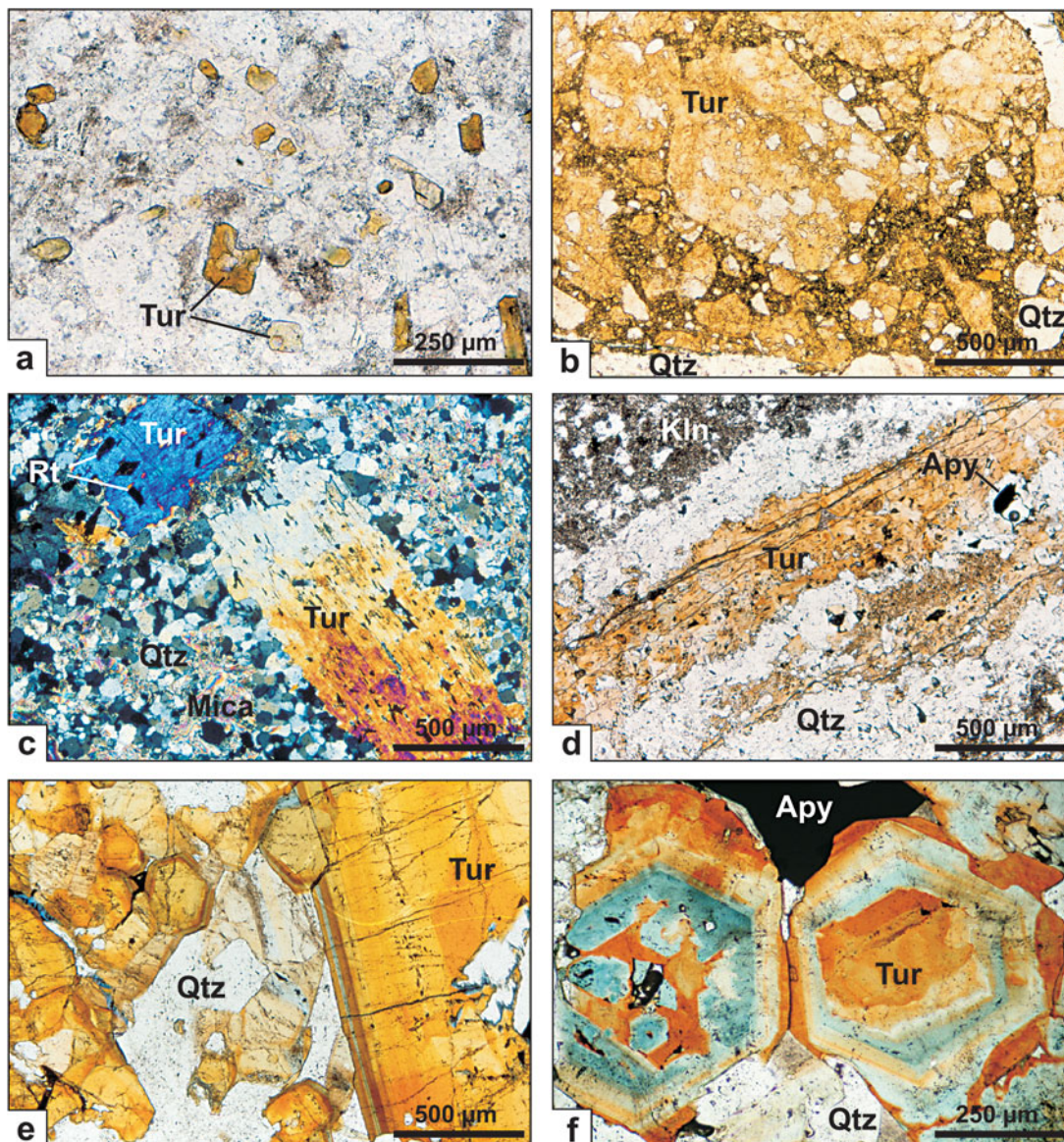


FIG. 3. a) Subhedral crystals of Fe-rich magmatic tourmaline (Tur) in a tourmaline leucogranite (sample I36). Plane-polarized light. b) Hydrothermal microbreccia composed of fragments of quartz (Qtz), tourmaline, and earlier tourmaline-quartz microbreccia, in a matrix of tourmalinized rock-flour. The microbreccia is cut by quartz veins and veinlets (sample SAR-A7). Plane-polarized light. c) Tourmalinized biotite laths with enclosed crystals of rutile (Rt) in a fine-grained matrix of altered granitic rock, composed of quartz and white mica (Mica) (sample I45). Crossed polars. d) Tourmaline-quartz veinlet with kaolinized (Kln) margins, cutting a tonalite. Rare arsenopyrite (Apy) crystals are disseminated in the veinlet (sample SAR-D3-47). Plane-polarized light. e) Color-zoned hydrothermal tourmaline, cut by veinlets of later blue tourmaline (center-left). Sample SAR-D1-280. Plane-polarized light. f) Complex color-zoning in vein tourmaline associated with quartz and arsenopyrite. Note the skeletal texture of the blue tourmaline (sample SAR-D1M-22). Plane-polarized light.

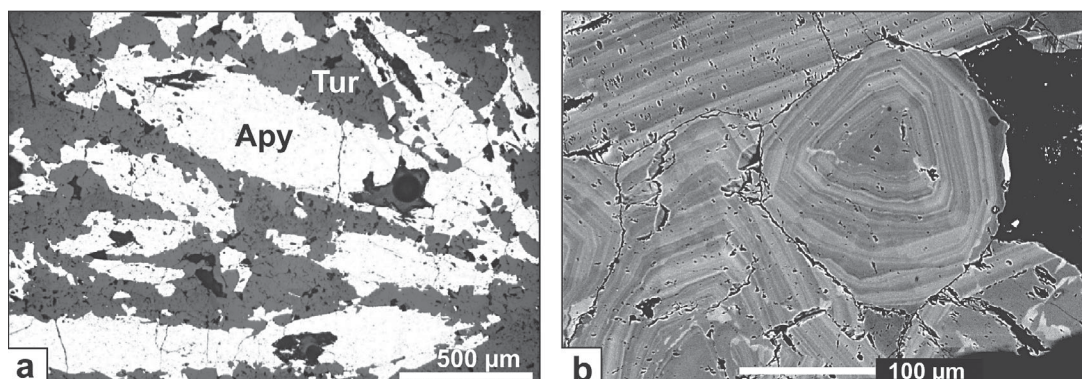


FIG. 4. a) Tourmaline intergrown with arsenopyrite (sample SAR–D3–39). Reflected light. b) Back-scattered-electron image of oscillatory zoning in hydrothermal tourmaline (orange dravite from the inset of Fig. 6d). Pale discordant zones in the lower part of the picture correspond to a later generation of light blue schorl. Sample SAR–D3–182.

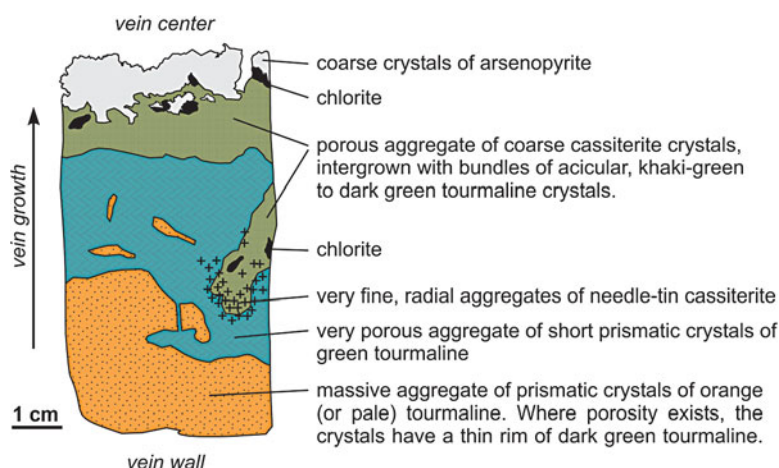


FIG. 5. Drawing of part of a mineralized vein showing the transition from early (orange or pale) tourmaline to late, dark green, iron-rich tourmaline, accompanied by cassiterite and chlorite, and followed by arsenopyrite (sample SAR–D3–182, Drill hole 3 through the Mariano vein, 182.5 m depth, elevation ~3967 m).

elbaite–liddicoatite corner), and none of the tourmaline compositions plots in the field of tourmaline from Lirich granites, as outlined by Henry & Guidotti (1985).

The pleochroic color of the tourmaline ($\omega \gg \epsilon$) correlates well with its major-element composition. Colorless tourmaline is Ti- and Fe-poor [<0.05 apfu Ti and $\text{Fe}/(\text{Fe} + \text{Mg}) < 0.30$], whereas yellow and orange varieties are Ti-rich (0.03–0.35 apfu Ti, Fig. 8). Orange tourmaline is also more Ca-rich than yellow tourmaline, with $\text{Na}/(\text{Na} + \text{Ca})$ values of less than 0.77 and 0.75–0.95, respectively. Blue and green varieties are poor in Ti, but relatively rich in Fe; the $\text{Fe}/(\text{Fe} + \text{Mg})$ value is between 0.40 and 0.75 for blue tourmaline, and

greater than 0.75 for the green variety. This correlation is very similar to that described from the Ore Knob massive sulfide deposit by Taylor & Slack (1984), who noted that blue and green tourmaline growth-zones have higher contents of Fe than yellow and brown growth-zones, which are enriched in Mg. A correlation between the pleochroic color of tourmaline and Ti content was also reported by Sinclair & Richardson (1992) for the Seagull batholith, Yukon Territory, where orange tourmaline is significantly more Ti-rich than blue tourmaline. Interestingly, both varieties of tourmaline from the latter locality are very Fe-rich [$\text{Fe}/(\text{Fe} + \text{Mg}) > 0.95$], suggesting that factors other than the concentra-

tion of Fe influence the color of tourmaline (*cf.* Faye *et al.* 1974, Slack & Coad 1989).

Figure 9 illustrates further compositional variations in the two datasets, for the complex tourmaline – cassiterite – chlorite – arsenopyrite vein (A), and the entire deposit (B). Values of $Fe/(Fe + Mg)$ plotted versus $X_{\square}/(Na + X_{\square})$ confirm the classification of most tourmaline samples as members of the dravite–schorl solid-solution series, as opposed to the alkali-deficient tourmaline series (Fig. 9a). This is also evident from an

Mg versus Fe plot (Fig. 9b), in which the bulk of the San Rafael tourmaline defines a compositional trend that corresponds closely to the dravite–schorl exchange vector $Mg^{2+} \leftrightarrow Fe^{2+}$ (*cf.* Burt 1989). There is, however, a systematic departure toward alkali-deficient tourmaline and oxy-tourmaline, which is due to the occurrence of additional elements, such as Al, at the Y site. It is noteworthy that the composition of the Fe-rich schorl defines a trend that is broadly parallel to the povondraite substitution-vector ($Fe^{3+} \leftrightarrow Al^{3+}$). This trend

TABLE 1. AVERAGE COMPOSITION OF TOURMALINE FROM SAN RAFAEL, PERU

Stage	magm.	v. early	v. early	v. early	early	early	early	early	early	trans.?	early
Tur type	magm.	alt.	alt.	alt.	alt.	alt.	alt.	alt.	alt.	vein	vein
Description of	dissem.	radiating	color-	color-	color-	aggreg.	repl.	radiating	zoned	late	over-
xls	equant	columnar	zoned	zoned	zoned	columnar	of Bt	columnar	columnar	growths	of Bt
Color (PPL)	dark yellow	colorless	dark yellow	blue	yellow	yellow	yellow	v. light blue	dark yellow	dark blue	pale yellow
Elev. (m)	5100	4950	4950	4950	4220	4050	4050	4050	4035	4035	4245
Assoc. minerals	Qtz, Pl, mica	Qtz, mica, Rt	Qtz, mica, Rt, Dum, Tur	Qtz, mica, Rt, Dum, Tur	Qtz, Rt, Ap	Qtz, Rt	Qtz, mica, Rt	Qtz, mica, Rt	Qtz, mica, Chl	Qtz, mica, Chl	Qtz, Rt
Sample	I36	I46	I46	I46	D4-94	J26A	J26C	J26C	D1-280	D1-280	D4-68A
SiO ₂ wt.%	34.53	37.07	35.33	36.08	36.34	36.25	36.23	36.83	35.96	35.65	36.10
TiO ₂	0.51	0.11	1.33	0.32	0.42	1.31	1.02	0.01	2.93	0.02	0.21
Al ₂ O ₃	35.11	38.66	32.07	32.82	35.29	30.82	33.00	33.58	29.85	33.21	35.64
Cr ₂ O ₃	n.a.	0.03	0.04	0.01	0.01	0.04	0.04	0.00	n.a.	n.a.	0.02
FeO	10.84	0.29	9.15	7.81	5.92	5.90	6.50	4.86	2.21	13.33	4.08
MnO	0.06	0.01	0.07	0.04	0.01	0.01	0.01	0.02	0.01	0.01	0.01
MgO	2.26	7.07	4.87	5.75	5.29	7.53	6.26	7.25	10.04	1.93	6.35
CaO	0.15	0.19	0.66	0.33	0.35	0.93	0.62	0.40	1.25	0.02	0.52
Na ₂ O	1.96	1.67	2.05	2.14	1.82	2.08	1.90	2.20	2.21	1.42	1.87
K ₂ O	0.05	0.02	0.06	0.05	0.03	0.04	0.09	0.03	0.03	0.01	0.03
F	0.37	0.24	0.60	0.65	0.29	0.20	0.51	0.09	0.18	0.04	0.36
Cl	n.a.	0.00	0.01	0.01	0.00	0.00	0.00	0.00	n.a.	n.a.	0.01
O=F,Cl	-0.16	-0.10	-0.25	-0.28	-0.12	-0.09	-0.21	-0.04	-0.08	-0.02	-0.16
Total	85.68	85.27	85.98	85.75	85.65	85.03	85.96	85.25	84.59	85.63	85.05
B <i>apfu</i>	3.000	3.000	3.000	3.000	3.000	3.000	3.000	3.000	3.000	3.000	3.000
Si	5.834	5.944	5.946	6.003	5.983	6.057	5.993	6.050	5.981	6.018	5.941
Al	6.992	7.307	6.362	6.435	6.846	6.070	6.431	6.502	5.852	6.609	6.912
Ti	0.064	0.014	0.168	0.041	0.052	0.165	0.127	0.001	0.368	0.003	0.026
Fe	1.532	0.039	1.288	1.088	0.817	0.825	0.899	0.668	0.307	1.882	0.561
Mn	0.009	0.002	0.010	0.006	0.002	0.002	0.001	0.003	0.002	0.001	0.001
Mg	0.569	1.691	1.221	1.427	1.299	1.875	1.543	1.775	2.491	0.487	1.558
Cr	n.a.	0.004	0.005	0.001	0.001	0.006	0.005	0.001	n.a.	n.a.	0.002
Ca	0.028	0.033	0.119	0.059	0.063	0.166	0.111	0.071	0.223	0.003	0.092
Na	0.641	0.518	0.670	0.692	0.580	0.674	0.609	0.701	0.712	0.464	0.595
K	0.010	0.004	0.014	0.011	0.006	0.008	0.019	0.006	0.007	0.003	0.007
□	0.322	0.445	0.197	0.238	0.352	0.152	0.261	0.223	0.059	0.530	0.306
Σ cations	15.678	15.555	15.803	15.762	15.648	15.848	15.739	15.777	15.941	15.470	15.694
F	0.199	0.122	0.317	0.342	0.150	0.108	0.266	0.045	0.095	0.020	0.190
Cl	n.a.	0.001	0.002	0.004	0.001	0.001	0.001	0.001	n.a.	n.a.	0.004
Fe/(Fe+Mg)	0.73	0.02	0.51	0.43	0.39	0.31	0.37	0.27	0.11	0.80	0.26
Na/(Na+Ca)	0.96	0.94	0.85	0.92	0.91	0.81	0.85	0.91	0.76	0.99	0.87
# of anal.	7	8	8	11	10	5	5	5	14	4	10

suggests that part of the iron in this tourmaline could be Fe³⁺ substituting for Al at the Z site, an interpretation re-inforced by the marked negative correlation between Al and Fe for this variety of tourmaline (Fig. 9c).

The relationship between Al content and X_{\square} shows the relative importance of the exchange mechanisms $\square\text{Al}(\text{NaR})_{-1}$, $\text{AlO}[\text{R}(\text{OH})]_{-1}$, and FeAl_{-1} (Fig. 9d). The substitution $\square\text{Al}(\text{NaR})_{-1}$, which depends strongly on the bulk concentration of Na in the system and on temperature (von Goerne *et al.* 2001), clearly dominated, especially in the late, Fe-rich varieties of tourmaline. A minor uvite component is apparent for the Ca-, Mg-, and F-enriched colorless and orange varieties of tourmaline from the multistage vein of set A (Figs. 9b, e).

The results of Fe²⁺/Fe³⁺ determinations using wet-chemical methods are presented in Table 2. Although they are semiquantitative at best, they establish that >50% of the iron present in the tourmaline samples is in the ferrous form and, therefore, the Fe-rich tourmaline represents schorl and not buergerite (a rare variety of ferric tourmaline). In addition, there is an indication that the latest generation of tourmaline, *i.e.*, the most Fe-rich, has a higher proportion of ferric iron than earlier tourmaline. This observation needs to be confirmed by more reliable methods.

Tin and tungsten in tourmaline

Tourmaline is a potential host for tin and tungsten through substitution of these elements at the Y site (Power 1968, Němec 1973). Tourmaline from several samples was analyzed for Sn and W by electron microprobe. The majority of the tourmaline crystals have a very low Sn content (<0.03 wt.% Sn). However, paragenetically late Fe-rich tourmaline (schorl) associated with cassiterite contains between 0.20 and 0.38 wt.% Sn (or up to 0.034 *apfu* Sn; Fig. 9f). These values are among the highest recorded for tourmaline, the other high values being: 0.46 wt.% Sn at Kidd Creek, Ontario (Slack *et al.* 1999); 0.35 wt.% Sn at Roche, southwest England (Williamson *et al.* 2000), and 0.42 wt.% Sn at Yunlong, China (Yu & Jiang 2003). On the basis of the relatively uniform distribution of Sn in the San Rafael tourmaline, as shown by electron-microprobe X-ray mapping (Fig. 10f), we conclude that the substantial amount of tin detected is present within the structure of the tourmaline (probably at the Y site), and does not represent inclusions of cassiterite. In contrast to Sn, the W content of San Rafael tourmaline is very low, typically <0.03 wt.% WO₃. In rare cases, it may reach 0.14 wt.% W (~0.01 W *apfu*).

Chemical evolution of zoned schorl

An investigation of the multistage tourmaline – cassiterite – chlorite – arsenopyrite veins (Fig. 5)

reveals that the large crystals of very Fe-rich tourmaline, which coexist with coarse cassiterite, exhibit strong color-zoning and compositional variations. One such crystal, ~1 mm long, was selected for detailed elemental X-ray mapping under the electron microprobe, and another was analyzed along a line profile traversing the successive growth-zones. The results shown in Figures 10 and 11 indicate that the orange-pleochroic core of these crystals is strongly enriched in Mg and that the overgrowth, which changes color progressively outward from bluish to dark green, is correspondingly enriched in Fe. This enrichment in Fe from core to overgrowth is sharp [Fe/(Fe + Mg) from 0.20 to 0.85] and coincides with enrichments in Sn (up to ~0.4 wt.%) and Na, and depletions in Ca, F, and Ti (Fig. 11). It should also be noted that the composition of the Mg-rich core matches closely that of the orange-colored tourmaline, which occurs earlier in the profile of the same vein (Fig. 5). The zoned crystals of tourmaline record a crucial part of the fluid history of the San Rafael deposit, reflecting the transition from the early, barren hydrothermal stage to the onset of cassiterite deposition.

DISCUSSION

The association of tourmaline with tin deposits

Tourmaline is a relatively common gangue mineral in many granite-related Sn–W hydrothermal systems, owing to the high concentration of boron in peraluminous felsic magmas (Taylor 1979, Barth 1988, Manning 1991, Linnen & Williams-Jones 1994, London & Manning 1995, LeBoutillier *et al.* 2002). Pichavant (1981) and Pichavant & Manning (1984) have shown that boron enrichment of silicate melts increases H₂O solubility, thereby lowering solidus temperatures and allowing more time for differentiation. Prolonged fractionation of crystals, in turn, favors the concentration of high-field-strength elements, notably tin, in the residual melt. In addition, the greater solubility of H₂O in B-rich magmas delays separation of an aqueous fluid until the ascent of magma to shallower levels and, therefore, lower confining pressures. The resulting volume expansion during “degassing” of the residual melts produces large fluid overpressures and the release of a great amount of mechanical energy. This, in turn, produces intense fracturing and brecciation, which lead to a greater focusing of the ore fluids and concentration of mineralization, as opposed to F-rich, greisen-style systems that are characterized by more passive crystallization and a more disseminated style of mineralization (Pollard *et al.* 1987, Halls 1994). These effects are very obvious at San Rafael, where the early, barren tourmaline–quartz veins established the primary framework of the vein–breccia system, which was subsequently reopened and mineralized with high-grade Sn (Mlynarczyk *et al.* 2003).

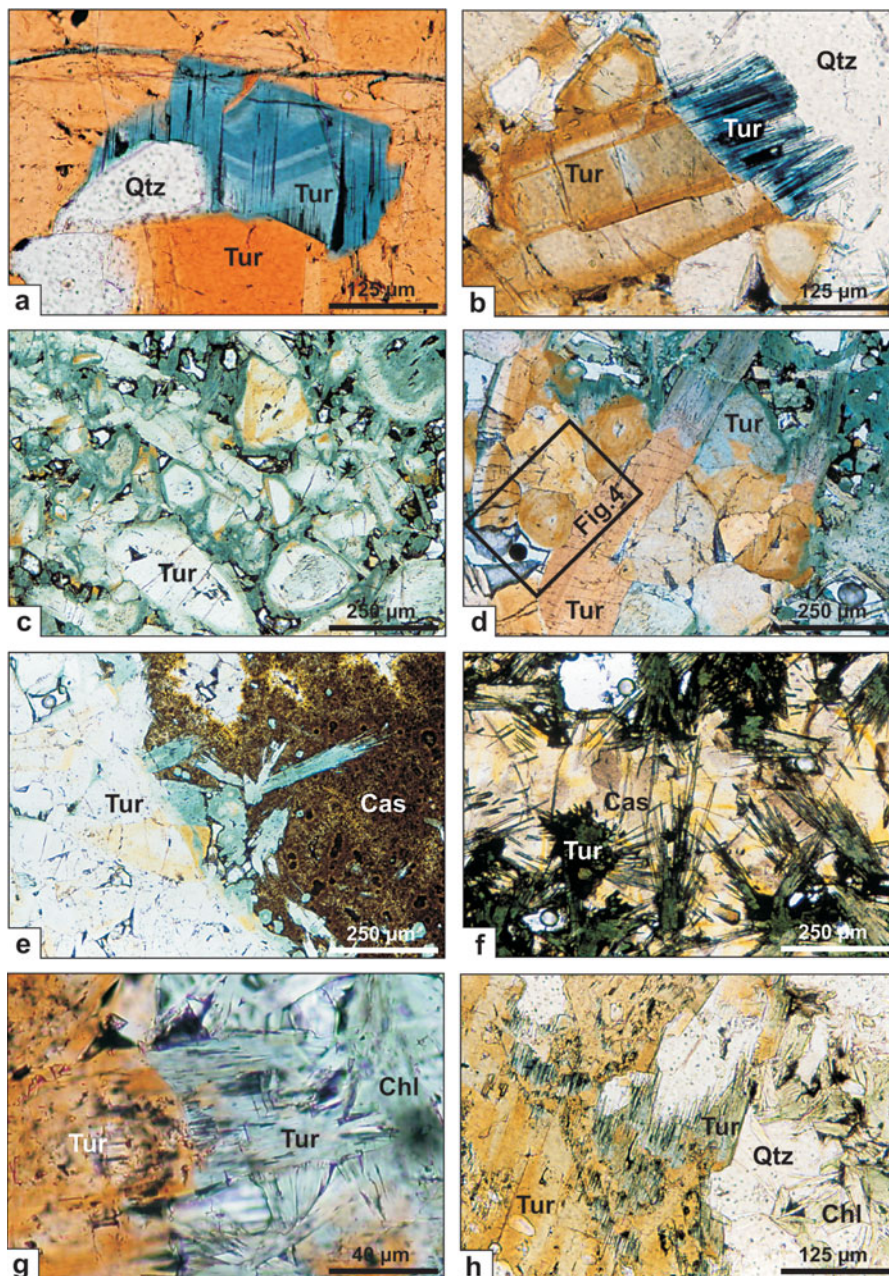


FIG. 6. a) Second generation of zoned, blue, iron-rich tourmaline (Tur), forming an overgrowth on orange, dravitic, vein tourmaline (sample SAR-D1-280). Plane-polarized light. b) Overgrowth of blue tourmaline on earlier dravite (yellow), in a tourmaline-quartz (Qtz) vein (sample SAR-D4-253). Plane-polarized light. c, d) Schorl (pale blue, green) overgrowth on dravite (colorless-yellow-orange) in a hydrothermal vein (sample SAR-D3-182). Plane-polarized light. e) Finely crystalline wood tin cassiterite (Cas), associated with schorl (green), which replaced and grew on earlier dravite (colorless-yellow) (sample SAR-D3-182). Plane-polarized light. f) Coarsely crystalline cassiterite, intimately intergrown with acicular schorl (khaki green to dark green). White patches represent voids in the sample. (sample SAR-D3-182). Plane-polarized light. g) Overgrowth of Fe-rich tourmaline (schorl ?) on earlier dravite (orange), coexisting with Fe-rich chlorite (Chl) (sample SAR-R-577, from a zone of intense, main-stage chloritic alteration). Plane-polarized light. h) Overgrowth of Fe-rich tourmaline (schorl ?) on earlier dravite (dark yellow), coexisting with quartz and main-stage chlorite (sample SAR-R14, from a zone of intense chloritic alteration). Plane-polarized light.

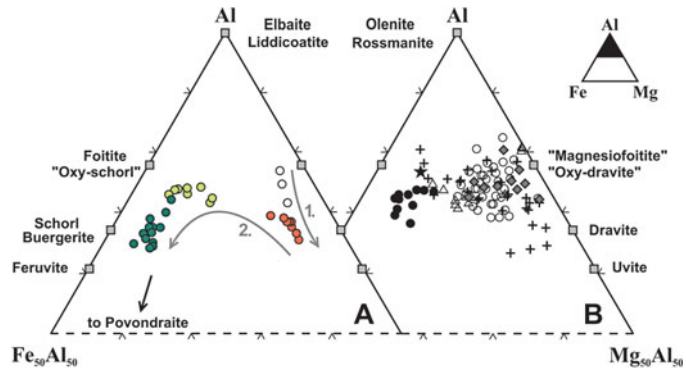
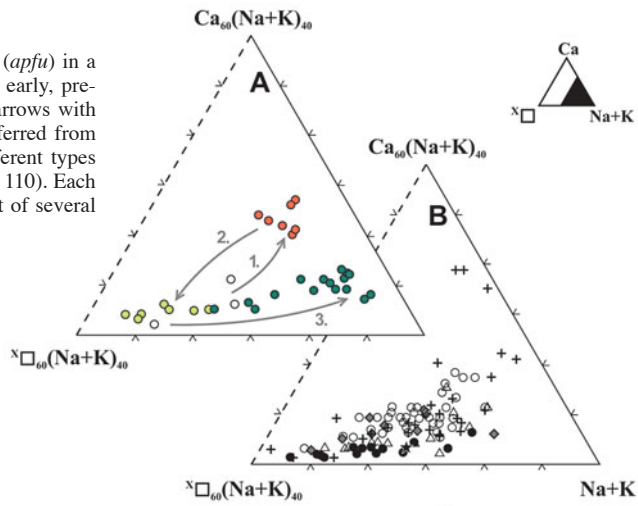


FIG. 7. A. Evolution of tourmaline composition (*apfu*) in a single vein (sample SAR-D3-182), from the early, pre-ore to the main tin-ore stages ($n = 41$). The arrows with numbers show the order of crystallization, inferred from vein textures (Fig. 5). B. Composition of different types of tourmaline from the San Rafael deposit ($n = 110$). Each point in the plots represents the average result of several electron-microprobe analyses.



A

- colorless vein tourmaline (1st gen.)
- orange vein tourmaline (2nd gen.)
- green vein tourmaline (3rd gen.)
- dark green vein tourmaline (4th gen.)

B

- ★ magmatic tourmaline
- ◆ tourmaline from microbreccia
- △ very early, alteration tourmaline
- early alteration tourmaline
- + vein tourmaline
- late overgrowths on earlier tourmaline

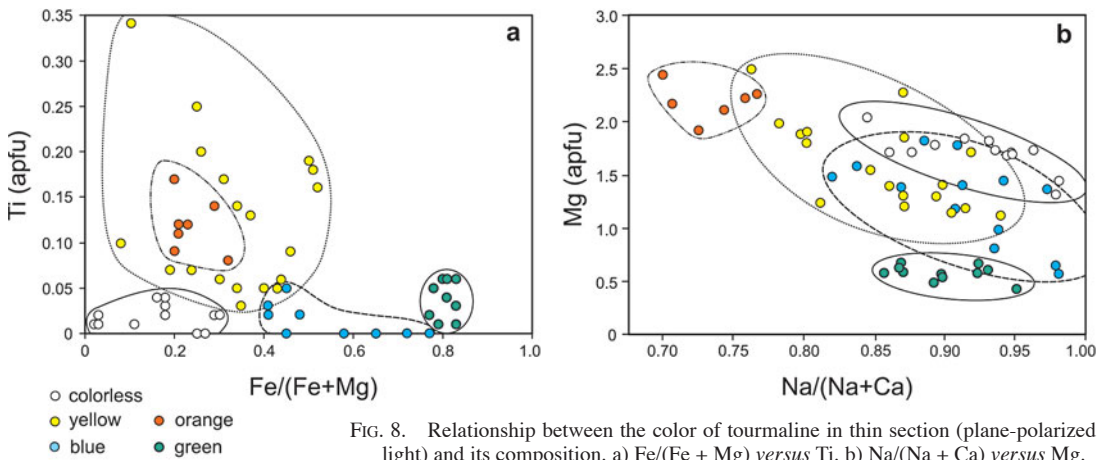


FIG. 8. Relationship between the color of tourmaline in thin section (plane-polarized light) and its composition. a) $Fe/(Fe + Mg)$ versus Ti . b) $Na/(Na + Ca)$ versus Mg .

Iron in tourmaline from granitic systems

Whereas tourmaline associated with sedimentary and metamorphic rocks is commonly rich in Mg, tourmaline from granitic environments is typically rich in Fe (Henry & Guidotti 1985), in particular tourmaline associated with tin mineralization. For example, Pirajno & Smithies (1992) noted that in the case of granite-related Sn–W deposits in South Africa, Namibia, and New Zealand, the Fe/(Fe + Mg) value of tourmaline increases from <0.6 for distal deposits to ~1 for proximal and endogranitic deposits. Significantly, as at San Rafael, the early, pre-ore tourmaline of granite-related Sn–W deposits is typically Mg-rich, whereas ore-stage tourmaline is Fe-rich, commonly with elevated concentrations of Sn (Emond 1985, Barth 1988, Griffin *et al.* 1996, Williamson *et al.* 2000, LeBoutillier *et al.* 2002). The opposite trend, with Mg-rich tourmaline associated with cassiterite ores, is observed only rarely, in distal deposits restricted to unusual geological settings (*e.g.*, the metamorphic Yunlong tin deposit, China: Yu & Jiang 2003).

The marked enrichment in iron of tourmaline from tin deposits matches the observation that in many suites of granitic rocks, including granitic pegmatites, the most fractionated members of the suite, *i.e.*, those with the greatest potential for associated enrichment in tin (Lehmann 1990), host the most iron-rich tourmaline (Power 1968, Neiva 1974, Manning 1982, Broska *et al.* 1998, Sinclair & Richardson 1992). The parallel geochemical behavior of tin and iron in hydrothermal fluids exsolved from highly evolved, fractionated magmas is most likely the result of both metals being effectively transported as chloride complexes in hot, reducing, relatively acidic and saline solutions (Eugster & Wilson 1985, Pabalan 1986, Heinrich 1990, Wood & Samson 1998, Müller & Seward 2001). Therefore, the magmatic brines responsible for the formation of tin deposits are likely to be very iron-rich.

Compositional trends in San Rafael tourmaline

The tourmaline at San Rafael is similar to hydrothermal tourmaline in granite-related Sn systems elsewhere in that it has ubiquitous color and compositional zoning, a relatively wide range of Fe and Mg contents, and a low F content (*cf.* London & Manning 1995). Like tourmaline in other tin deposits, San Rafael tourmaline is also rich in Al (Fig. 9c), especially where it occurs as a product of alteration, consistent with the fact that the precursor granitic rocks have a strongly peraluminous bulk-composition (*cf.* Manning 1991). The most outstanding feature of the San Rafael tourmaline, however, is the very high Fe content of the late generation of schorl. In this respect, the schorl from San Rafael is similar to some of the late tourmaline from the Cornish tin deposits that is commonly referred to as “blue peach” (Farmer & Halls 1993).

Power (1968) described the occurrence there of zoned acicular crystals of blue-green tourmaline, which grew locally on corroded nuclei of an earlier, yellow-brown generation of tourmaline (*cf.* Fig. 10a). More recently, Williamson *et al.* (2000) reported overgrowths of a blue, Fe- and Sn-rich tourmaline on an earlier, light brown, Mg- and F-rich tourmaline from fault breccias at Roche, southwestern England (the oxidation state of iron in the tourmaline from those localities was not determined analytically, but the authors infer that the Fe-rich varieties are schorl). Understanding the formation of the late schorl at San Rafael can, therefore, provide an important insight into the fluid evolution and ore deposition not only at this world-class deposit, but also in hydrothermal tin lodes elsewhere.

The remarkable feature of the Fe-rich schorl at San Rafael is that its appearance in the paragenesis was quite abrupt, and directly preceded the large-scale precipitation of cassiterite, with which it is finely intergrown. Thus, the multistage tourmaline – cassiterite – chlorite – arsenopyrite veins described above record marked changes in mineral assemblage and mineral composition. The color of the precipitating tourmaline (as seen in plane-polarized light) changed abruptly from colorless and orange to green, and subsequently dark green, whereas its composition became strongly Fe-rich, as well as enriched in Sn. On the basis of a strong correlation between the concentrations of Sn and Fe in this tourmaline (Fig. 9f), we conclude that Sn and Fe were incorporated into its structure during crystallization from an Fe-rich, cassiterite-saturated ore fluid. This interpretation is consistent with the tendency of tourmaline to incorporate trace elements in proportion to their concentration in the hydrothermal fluid (Griffin *et al.* 1996, Slack *et al.* 1999). From the conspicuous partial dissolution of the orange magnesian tourmaline (Fig. 10a), it is also evident that the fluid that deposited schorl and cassiterite was not in equilibrium with the early generation of tourmaline. The composition of tourmaline at San Rafael, therefore, recorded the abrupt physicochemical changes in the hydrothermal fluid that triggered ore deposition.

Significance of tourmaline zoning for fluid evolution at San Rafael

The hydrothermal system at San Rafael clearly experienced two different stages of fluid evolution, expressed by contrasting styles of veining, alteration, and mineralogy. Whereas the early, barren tourmaline–quartz veins are invariably narrow, sealed, and typically discontinuous, indicating that they formed under lithostatic conditions, the ore veins show evidence of open-space filling and must have formed under largely hydrostatic conditions. This conspicuous difference in vein character is paralleled by a marked change in alteration style (from white mica alteration and tourmaline alteration to strong chloritic alteration),

and a change in the physicochemical conditions of the ore fluids. Mlynarczyk *et al.* (2006a, b) established that the fluids characterizing the early, barren hydrothermal stage were high-temperature, hypersaline brines ($535 < T_h < 240^\circ\text{C}$, 34–62 wt.% NaCl eq.; Fig. 2). Using the isocon method of Grant (1986) and a normalization to Ti, Mlynarczyk *et al.* found that these brines leached the bulk of alkali and alkaline-earth elements from granitic precursors, and produced a gain of B of >10,000% relative to its concentration in the fresh rock (*i.e.*, >100-fold), as well as gains in Mg of 75% and Fe of ~40%. By contrast, the ore-stage fluids were of only moderate temperature and moderate to low salinity ($361 < T_h < 265^\circ\text{C}$, 0.5–21 wt.% NaCl eq., Fig. 2). Although they too strongly leached alkali and alkaline-earth elements from the wallrocks, these ore fluids produced a much larger gain of Fe than the fluids that precipitated tourmaline, typically between 2 and 5 fold (200–500%). In addition, chloritic alteration was accompanied by a 300 to 2,000% mass gain in Sn, a 100 to 2,300% mass gain in W, a 220 to 350% mass gain in Mn, a 100 to 330% mass gain in H_2O , and a mass gain of up to 35% in Mg, relative to their concentrations in the fresh rocks (Mlynarczyk *et al.* 2006a). The obvious question, therefore, is whether the two genetic stages were related, and if so, what physicochemical changes led to the second (mineralizing) stage.

Important clues about the relationship between these stages and the changing physicochemical conditions are offered by the tourmaline – cassiterite – chlorite – arsenopyrite veins. These peculiar veins contain abundant tourmaline, implying that they represent the early, barren stage of the hydrothermal system, yet they show open-space filling textures, are surrounded by a halo of strong chloritic alteration, and contain cassiterite, *i.e.*, they also represent the ore stage. Furthermore, these two stages are clearly reflected in the abrupt change from orange to late bluish to green tourmaline. Such features suggest that the main ore-stage followed shortly after the early barren stage, and that formation of the tourmaline – cassiterite – chlorite – arsenopyrite veins overlapped the barren and ore stages. More importantly, these veins mark the onset of cassiterite and chlorite precipitation, and record a major change in fluid composition that accompanied mineralization (evidenced by the strong increase in the iron content of tourmaline and the sharp change of its color). The fact that these changes were associated with a markedly different vein-style, *i.e.*, the first occurrence of open-space filling in the deposit paragenesis, implies that the onset of tin mineralization at San Rafael was brought about by a dramatic change in the plumbing of the hydrothermal system. We infer that a transition from a closed system (lithostatic conditions) to an open system (hydrostatic conditions) took place at that time. The hypothesis of a sudden “opening” of the hydrothermal system inevitably raises the possibility of fluid boiling and an influx of external fluids, both of which are very

efficient mechanisms for triggering ore deposition. The lack of fluid-inclusion evidence for boiling, together with the involvement of increasingly dilute and colder fluids (Fig. 2), and the stable isotope compositions of ore and gangue minerals (Mlynarczyk *et al.* 2006b), strongly suggest the latter scenario, and point to fluid mixing as the cause of tin mineralization.

The transition from the pre-ore (tourmalinization) stage to the ore stage was probably abrupt, as deduced from the corrosion of the Mg-rich core of tourmaline prior to the crystallization of schorl (Fig. 10a), and from the strong enrichment in iron of successive

TABLE 2. ANALYZED CONCENTRATION OF FERRIC AND FERROUS Fe IN SELECTED TOURMALINE SEPARATES FROM SAN RAFAEL

Sample	Macroscopic description of the tourmaline	FeO	Fe ₂ O ₃	Fe ₂ O ₃ 100Fe ³⁺ total / ΣFe
A7	light reddish brown, in breccia	1.73	0.70	2.62 27
R533	dark brown, in breccia	1.65	1.40	3.23 43
R507-A	dark brown, in breccia	1.97	1.22	3.41 36
R507-B*	creamy-greyish, euhedral, in breccia	2.31	2.07	4.64 45
D3-208	dark brown, in vein	3.09	2.12	5.55 38
D5-135	dark brown, in vein	3.44	0.62	4.44 14
J26-A	brown-greyish, as alteration	2.75	1.30	4.36 30
D5-138-A	brown, locally euhedral, as alteration	1.28	1.16	2.58 45
D5-138-B*	greenish black, as cross-cutting veinlets	2.00	1.50	3.72 40
D4-94-A	light brown, as alteration	1.35	0.35	1.85 19
D4-94-B*	dark brown, as veinlets	1.85	1.48	3.54 42
D5-70	brown-grey, euhedral, in vein vugs	3.11	7.05	10.51 67
D1-303-A	orange-brown, in vein	2.39	0.79	3.45 23
D1-303-B*	blue, veinlets cross-cutting the former	2.08	1.34	3.65 37
D3-182A-2	orange, in vein	2.95	1.44	4.72 31
D3-182A-4	dark green, in vein	7.16	5.29	13.25 40
108796	dravite standard (titration)	5.09	10.40	16.06 65
	dravite standard (Mössbauer) ^{1,2,3}	6.56	8.56	15.84 54
	dravite standard (XANES) ²	–	–	– 62
112566	schorl standard (titration)	7.94	7.37	16.19 46
	schorl standard (Mössbauer) ^{1,2,3}	14.48	0.00	16.07 0
	schorl standard (XANES) ^{2,3}	–	–	– 0
STRGR-2	schorl standard (titration)	7.01	3.75	11.54 32
	schorl standard (Mössbauer) ^{1,3}	10.56	0.55	12.27 4
98144	elbaite standard (titration)	4.22	2.68	7.37 36
	elbaite standard (Mössbauer) ^{2,3}	5.12	1.25	6.93 18
	elbaite standard (XANES) ^{2,3}	–	–	– 25
BU-1	buergerite from Mexquitic (titration)	0.80	15.49	16.38 95
	buergerite from Mexquitic (titration) ⁴	1.27	17.62	19.03 93

Note: except for the standards, the FeO and Fe₂O₃ concentrations listed above, expressed in wt.%, are for mineral separates, composed of variable proportions of tourmaline and quartz, (depending on how easy it was to separate tourmaline from quartz). The data on ferric and ferrous iron quoted, however, represent the tourmaline, as it is the only Fe-bearing mineral in the separates.

According to electron microprobe analyses, the majority of the samples from San Rafael have the composition of dravite. Only D5-70 and D3-182A-4 represent schorl. The samples indicated with an asterisk (*) represent a second generation of vein tourmaline, which was so finely intergrown with the first generation that a small proportion of it is present in the sample. For all such samples (except D5-138B), the actual ferric iron content of the tourmaline is higher than that analyzed, as those separates were diluted by a tourmaline with a higher content of ferrous iron. As can be concluded from the analyses of the standards, the titration method used here gives a minimum estimate of the ferrous iron content in tourmaline (in the case of the two schorl standards, it underestimates the ferrous iron content very significantly).

Source of compositional data on the standards: (1) Dyar *et al.* (1998), (2) Dyar *et al.* (2001), (3) M.D. Dyar (pers. commun., 2004), (4) Donnay *et al.* (1966).

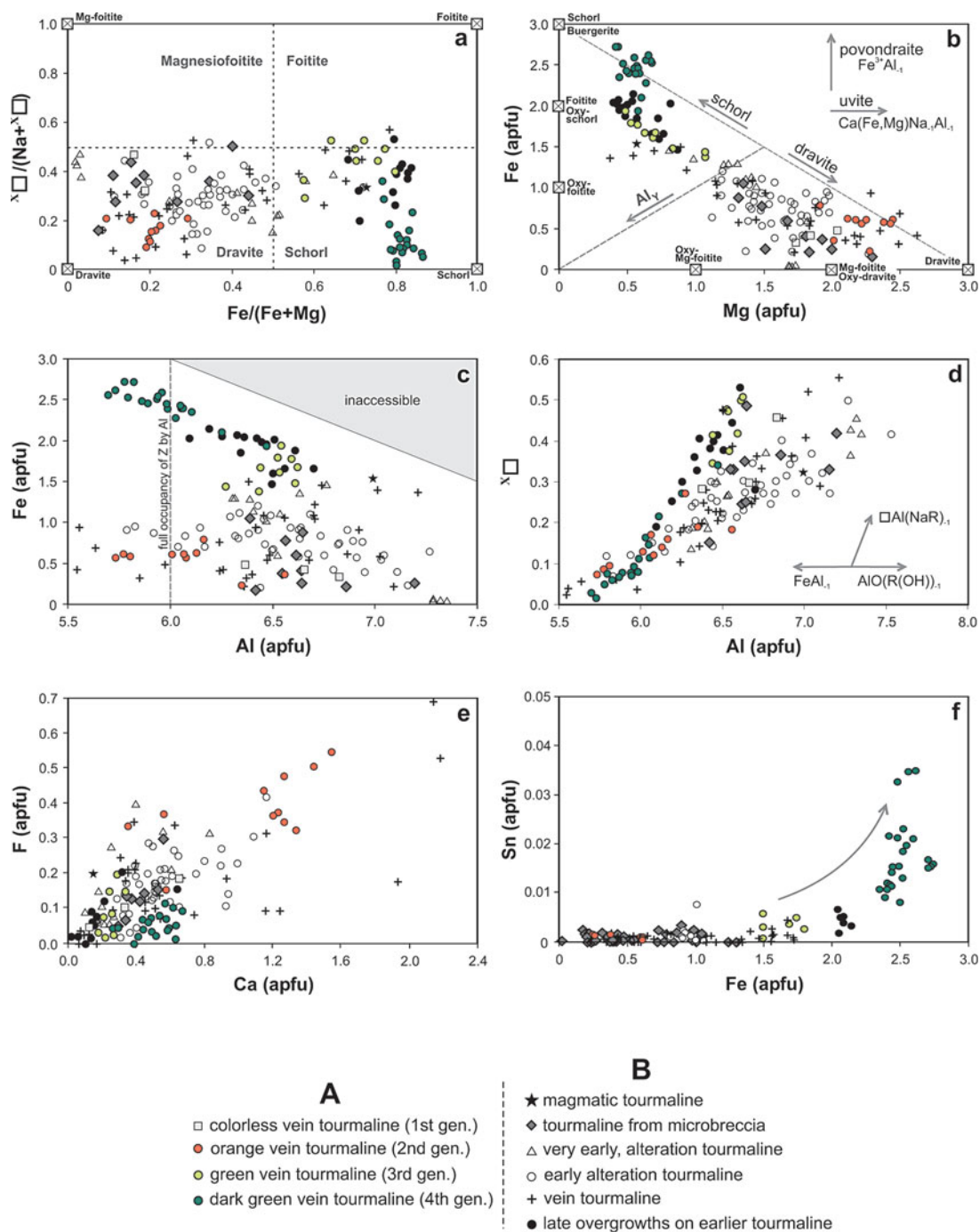


Fig. 9. Diagrams (a–f) showing the composition of tourmaline from: A. a single vein (sample SAR–D3–182), which records the transition from the early, barren to the main, tin-ore stage ($n = 41$); B. other parts of the San Rafael deposit ($n = 110$). Each point represents the average result of several electron-microprobe analyses, except for diagram f, which shows single analyses for a different set of data ($n = 126$). The plots show selected end-member compositions (small boxes) and substitution vectors (arrows). R in diagram c represents the sum of $Fe_{\text{(total)}} + Mg$.

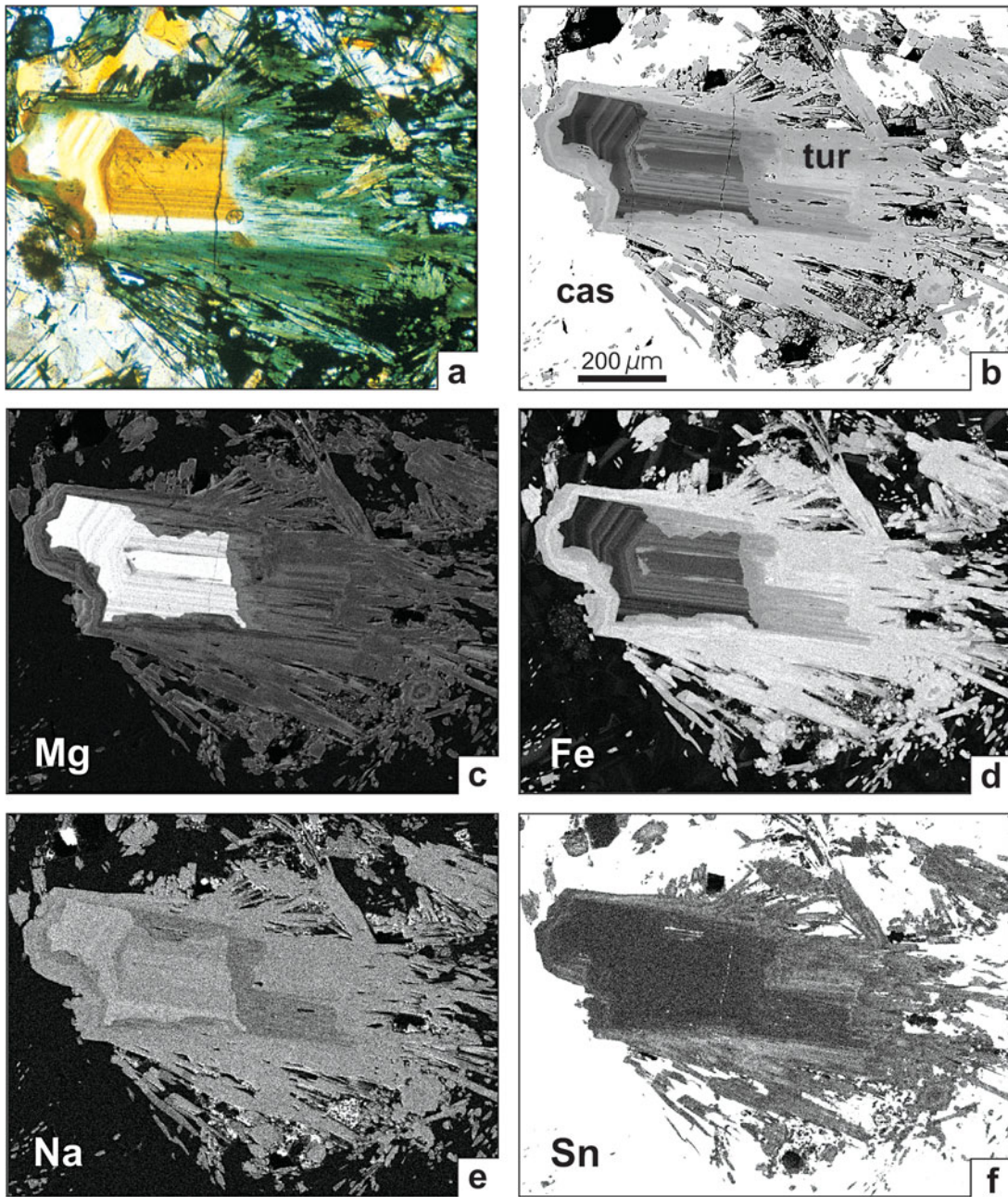


FIG. 10. (a) Color zoning in a crystal of hydrothermal tourmaline (center), intergrown with cassiterite. Sample D3-182, plane-polarized light. (b) Corresponding back-scattered-electron image. (c-f) X-ray element maps for Mg, Fe, Na, and Sn for the same crystal.

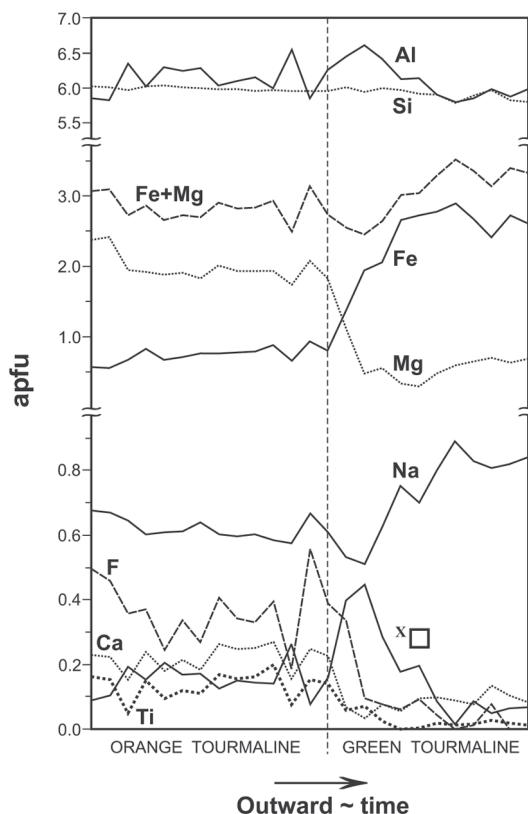


FIG. 11. Compositional zoning in a single crystal of tourmaline, recording the evolution from early, pre-ore to ore-stage tourmaline.

growth-zones (Fig. 11). The acicular habit of schorl coprecipitating with cassiterite, and the appearance of needle-tin (fine, acicular cassiterite), which preceded the deposition of coarser crystals of cassiterite, also indicate rapid crystallization and, hence, strong gradients in physicochemical conditions (supersaturation). The progressive increase in $Fe/(Fe + Mg)$ in tourmaline likely reflects the large decrease in temperature (500 to 300°C) that accompanied evolution of the hydrothermal system, and is consistent with calculations showing that the equilibrium constant for the reaction,



increases by over six orders of magnitude (*i.e.*, from $10^{-8.6}$ to $10^{-2.3}$) over this temperature interval (the pressure was assumed to be 500 bars).

The strong iron-enrichment of tourmaline, which preceded cassiterite deposition at San Rafael, therefore appears to reflect the cooling that resulted from fluid

mixing. We propose that a tectonic event took place during the evolution of the vein-breccia system, and opened the latter to an influx of externally derived fluids. Inasmuch as the emplacement of the San Rafael pluton was shallow, these fluids were most likely meteoric, an interpretation supported by their very low salinity (Mlynarczyk *et al.* 2006b). Also, the higher Fe^{3+}/Fe^{2+} value of the latest generation of tourmaline suggests that these fluids were oxidizing, consistent with the observation that Sn is dissolved predominantly as a Sn^{2+} -bearing chloride species (Eugster & Wilson 1985), but precipitates as Sn^{4+} in cassiterite. Thus, the mixing of hot tin- and iron-rich magmatic brines with dilute, cooler, and oxidizing meteoric waters not only caused the saturation of Fe-rich gangue minerals such as schorl and chlorite, but also provided a most efficient mechanism for the deposition of cassiterite (Heinrich 1990), leading to the formation of the world's richest tin ores.

CONCLUSIONS

Tourmaline is the dominant mineral in the early (pre-ore) paragenesis of the San Rafael tin deposit, and continued to crystallize until the onset of cassiterite precipitation. Although several varieties of tourmaline formed, there is a clearly recognizable, deposit-wide compositional trend from early Mg-rich (mostly dravite) to late Fe-rich tourmaline (schorl), which reflects a marked decrease in the temperature of crystallization. On the basis of structural evidence for opening of the vein system immediately prior to tin mineralization, as well as fluid-inclusion evidence, we conclude that the rich tin ores of San Rafael were the result of a sudden influx of cooler, dilute, oxidizing meteoric water into the hydrothermal system, and its mixing with tin- and iron-rich magmatic brines.

ACKNOWLEDGEMENTS

The authors thank Ing. Fausto Zavaleta Cruzado, General Manager of MINSUR S.A., Ing. Luis Alva Florian, manager of the San Rafael mine, and other mine staff for collaboration during field work. Many thanks go to David Dolejš for help in recalculating the results of electron-microprobe analyses of tourmaline and calculating the fluid-mineral equilibria. We also gratefully acknowledge Lang Shi for assisting with electron-microprobe analyses at McGill University, and Andrzej Kozłowski and Ewa Slaby from the Faculty of Geology of the University of Warsaw, Poland, for arranging additional electron-microprobe analyses of tourmaline. Finally, we thank Darby Dyar and Carl Francis for kindly providing reference tourmaline material. The manuscript benefitted from constructive reviews by J.F. Slack and E. Slaby and the efficient editorial handling of R.F. Martin. The research was supported by an NSERC Discovery grant to AEW-J.

REFERENCES

- ARENAS, M.J. (1980): Mapa geológico superficial del Distrito Minero San Rafael, Puno. MINSUR S.A. Archives.
- BARBARIN, B. (1999): A review of the relationships between granitoid types, their origins, and their geodynamic environments. *Lithos* **46**, 605-626.
- BARTH, W.H. (1988): Compositional variation of zoned tourmalines associated with Sn–W mineralisation. *Geol. Soc. Aust., Abstr.* **21**, 439-440.
- BOUVIER, J.-L., SEN GUPTA, J.G. & ABBEY, S. (1972): Use of an “automatic sulphur titrator” in rock and mineral analysis: determination of sulphur, total carbon, carbonate, and ferrous iron. *Geol. Surv. Can., Pap.* **72-31**.
- BROSKA, I., UHER, P. & LIPKA, J. (1998): Brown and blue schorl from the Spiš-Gemer granite, Slovakia: composition and genetic relations. *J. Czech Geol. Soc.* **43**(1/2), 9-16.
- BURT, D.M. (1989): Vector representation of tourmaline compositions. *Am. Mineral.* **74**, 826-839.
- CARLIN, J. (2005): Tin. *In Mineral Commodity Summaries. U.S. Geol. Surv., Periodic Publ.*, 174-175.
- CAVARETTA, G. & PUXEDDU, M. (1990): Schorl – dravite – feridravite tourmalines deposited by hydrothermal magmatic fluids during early evolution of the Larderello geothermal field, Italy. *Econ. Geol.* **85**, 1236-1251.
- CHAPPELL, B.W. & WHITE, A.J.R. (1974): Two contrasting granite types. *Pacific Geol.* **8**, 173-174.
- DONNAY, G., INGAMELLS, C.O. & MASON, B. (1966): Buergerite, a new species of tourmaline. *Am. Mineral.* **51**, 198-199.
- DYAR, M.D., TAYLOR, M.E., LUTZ, T.M., FRANCIS, C.A., GUIDOTTI, C.V. & WISE, M. (1998): Inclusive chemical characterization of tourmaline: Mössbauer study of Fe valence and site occupancy. *Am. Mineral.* **83**, 848-864.
- DYAR, M.D., WIEDENBECK, M., ROBERTSON, D., CROSS, L.R., DELANEY, J.S., FERGUSON, K., FRANCIS, C.A., GREW, E.S., GUIDOTTI, C.V., HERVIG, R.L., HUGHES, J.M., HUSLER, J., LEEMAN, W., MCGUIRE, A.V., RHEDE, D., ROTHE, H., PAUL, R.L., RICHARDS, I. & YATES, M. (2001): Reference minerals for the microanalysis of light elements. *Geostandards Newsletter* **25**, 441-463.
- EMOND, D.S. (1985): Geology, mineralogy and petrogenesis of tin-bearing breccias, Oliver Creek, McQuesten River area, Yukon Territory. *In Granite-Related Mineral Deposits; Geology, Petrogenesis and Tectonic Setting* (R.P. Taylor & D.F. Strong, eds.). *Can. Inst. Mining Metall., Spec. Vol.*, 116-119.
- EUGSTER, H.P. & WILSON, G.A. (1985): Transport and deposition of ore-forming elements in hydrothermal systems associated with granites. *In High Heat Production (HHP) Granites, Hydrothermal Circulation and Ore Genesis* (C. Halls, ed.). Institution of Mining and Metallurgy, London, U.K. (87-98).
- FARMER, C.B. & HALLS, C. (1993): Paragenetic evolution of cassiterite-bearing lodes at South Crofty mine, Cornwall, United Kingdom. *In Proc. 8th IAGOD Symp.* (Ottawa; Y. Maurice, ed.). E. Schweizerbart'sche Verlagsbuchhandlung, Stuttgart, Germany (365-382).
- FAYE, G.H., MANNING, P.G., GOSSELIN, J.R. & TREMBLAY, R.J. (1974): The optical absorption spectra of tourmaline: importance of charge-transfer processes. *Can. Mineral.* **12**, 370-380.
- GRANT, J.A. (1986): The isocon diagram – a simple solution to Gresen's equation for metasomatic alteration. *Econ. Geol.* **81**, 1976-1982.
- GRIFFIN, W.L., SLACK, J.F., RAMSDEN, A.R., WIN, T.T. & RYAN, C.G. (1996): Trace elements in tourmalines from massive sulfide deposits and tourmalinites: geochemical controls and exploration applications. *Econ. Geol.* **91**, 657-675.
- HALLS, C. (1994): Energy and mechanism in the magmato-hydrothermal evolution of the Cornubian batholith: a review. *In Metallogeny of Collisional Orogens* (R. Seltmann, H. Kämpf & P. Möller, eds.). Czech Geological Survey, Prague, Czech Republic (274-294).
- HAWTHORNE, F.C. & HENRY, D.J. (1999): Classification of the minerals of the tourmaline group. *Eur. J. Mineral.* **11**, 201-215.
- HEINRICH, C.A. (1990): The chemistry of hydrothermal tin (–tungsten) ore deposition. *Econ. Geol.* **85**, 457-481.
- HENRY, D.J. & DUTROW, B.L. (1996): Metamorphic tourmaline and its petrologic applications. *In Boron: Mineralogy, Petrology and Geochemistry* (E.S. Grew & L.M. Anovitz, eds.). *Rev. Mineral.* **33**, 503-557.
- HENRY, D.J. & GUIDOTTI, C.V. (1985): Tourmaline as a petrogenetic indicator mineral: an example from the staurolite-grade metapelites of NW Maine. *Am. Mineral.* **70**, 1-15.
- INGAMELLS, C.O. (1960): A new method for “ferrous iron” and “excess oxygen” in rocks, minerals, and oxides. *Talanta* **4**, 268-273.
- JIANG, SHAO-YONG, PALMER, M.R., SLACK, J.F. & SHAW, D.R. (1998): Paragenesis and chemistry of multistage tourmaline formation in the Sullivan Pb–Zn–Ag deposit, British Columbia. *Econ. Geol.* **93**, 47-67.
- LEBOUTILLIER, N.G., CAMM, G.S., SHAIL, R.K., BROMLEY, A.V., JEWSON, C. & HOPPE, N. (2002): Tourmaline – quartz – cassiterite mineralization of the Land's End Granite at Nanjizal, west Cornwall. *Proc. Ussher Soc.* **10**, 312-318.
- LEHMANN, B. (1979): Schichtgebundene Sn-Lagerstätten in der Cordillera Real, Bolivien. *Berliner Geowissenschaftliche Abhandlungen, Reihe A: Geologie und Palaeontologie* **14**.

- LEHMANN, B. (1990): *Metallogeny of Tin*. Springer-Verlag, Berlin, Germany.
- LINNEN, R.L. & WILLIAMS-JONES, A.E. (1994): The evolution of pegmatite-hosted Sn–W mineralization at Nong-Sua, Thailand: evidence from fluid inclusions and stable isotopes. *Geochim. Cosmochim. Acta* **58**, 735-747.
- LONDON, D. & MANNING, D.A.C. (1995): Chemical variation and significance of tourmaline from southwest England. *Econ. Geol.* **90**, 495-519.
- LYNCH, G. & ORTEGA, J. (1997): Hydrothermal alteration and tourmaline–albite equilibria at the Coxheath porphyry Cu–Mo–Au deposit, Nova Scotia. *Can. Mineral.* **35**, 79-94.
- MANNING, D.A.C. (1982): Chemical and morphological variation in tourmalines from the Hub Kapong batholith of peninsular Thailand. *Mineral. Mag.* **45**, 139-147.
- MANNING, D.A.C. (1991): Chemical variation in tourmalines from south–west England. *Proc. Ussher Soc.* **7**, 327-332.
- MLYNARCZYK, M.S.J., SHERLOCK, R.L. & WILLIAMS-JONES, A.E. (2003): San Rafael, Peru: geology and structure of the worlds richest tin lode. *Mineral. Deposita* **38**, 555-567.
- MLYNARCZYK, M.S.J., WAGNER, T., WILLIAMS-JONES, A.E. & BOYCE, A.J. (2006b): Stable isotope constraints on ore formation at the San Rafael cassiterite-sulfide deposit, SE Peru. *Mineral. Deposita* (in press).
- MLYNARCZYK, M.S.J., WILLIAMS-JONES, A.E. & DOLEJŠ, D. (2006a): Geology and geochemistry of alteration at the San Rafael Sn–Cu deposit, SE Peru. *Econ. Geol.* (in press).
- MÜLLER, B. & SEWARD, T.M. (2001): Spectrophotometric determination of the stability of tin(II) chloride complexes in aqueous solution up to 300°C. *Geochim. Cosmochim. Acta* **65**, 4187-4199.
- NEIVA, A.M.R. (1974): Geochemistry of tourmaline (schorlrite) from granites, aplites and pegmatites from northern Portugal. *Geochim. Cosmochim. Acta* **38**, 1307-1317.
- NĚMEC, D. (1973): Tin in tourmalines. *Neues Jahrb. Mineral., Monatsh.*, 58-63.
- NOVÁK, M. (1998): Blue dravite as an indicator of fluid composition during subsolidus replacement processes in Li-poor granitic pegmatites in the Moldanubicum, Czech Republic. *J. Czech Geol. Soc.* **43**(1/2), 24-30.
- PABALAN, R.T. (1986): *Solubility of Cassiterite (SnO₂) in NaCl Solutions from 200°C – 350°C, with Geologic Applications*. Ph.D. thesis, Pennsylvania State University, University Park, Pa.
- PICHAVANT, M. (1981): An experimental study of the effect of boron on a water-saturated haplogranite at 1 kbar vapour pressure. *Contrib. Mineral. Petrol.* **76**, 430-439.
- PICHAVANT, M. & MANNING, D. (1984): Petrogenesis of tourmaline granites and topaz granites: the contribution of experimental data. *Phys. Earth Planet. Interiors* **35**, 31-50.
- PIRAJNO, F. & SMITHIES, R.H. (1992): The FeO/(FeO+MgO) ratio of tourmaline: a useful indicator of spatial variations in granite-related hydrothermal mineral deposits. *J. Geochem. Explor.* **42**, 371-381.
- POLLARD, P.J., PICHAVANT, M. & CHAROY, B. (1987): Contrasting evolution of fluorine- and boron- rich tin systems. *Mineral. Deposita* **22**, 315-321.
- POVONDRA, P. & ČECH, F. (1976): A method for the chemical analysis of tourmalines. *Acta Universitatis Carolinae – Geologica* **3**, 209-217.
- POVONDRA, P. & ULRYCH, J. (1976): A contribution to the methods for the determination of divalent iron in amphiboles. *Acta Universitatis Carolinae – Geologica* **2**, 85-89.
- POWER, G.M. (1968): Chemical variation in tourmalines from south–west England. *Mineral. Mag.* **36**, 1078-1089.
- SINCLAIR, W.D. & RICHARDSON, J.M. (1992): Quartz–tourmaline orbicules in the Seagull batholith, Yukon Territory. *Can. Mineral.* **30**, 923-935.
- SLACK, J.F. (1996): Tourmaline associations with hydrothermal ore deposits. In *Boron: Mineralogy, Petrology and Geochemistry* (E.S. Grew & L.M. Anovitz, eds.). *Rev. Mineral.* **33**, 559-643.
- SLACK, J.F. & COAD, P.R. (1989): Multiple hydrothermal and metamorphic events in the Kidd Creek volcanogenic massive sulphide deposit, Timmins, Ontario: evidence from tourmalines and chlorites. *Can. J. Earth Sci.* **26**, 694-715.
- SLACK, J.F., RAMSDEN, A.R., GRIFFIN, W.L., WIN, T.T., FRENCH, D.H. & RYAN, C.G. (1999): Trace elements in tourmaline from the Kidd Creek massive sulfide deposit and vicinity, Timmins, Ontario: a proton microprobe study. In *The Giant Kidd Creek Volcanogenic Massive Sulfide Deposit, Western Abitibi Subprovince, Canada* (M.D. Hannington & C.T. Barrie, eds.). *Econ. Geol., Monogr.* **10**, 415-430.
- TAYLOR, B.E. & SLACK, J.F. (1984): Tourmalines from Appalachian–Caledonian massive sulfide deposits: textural, chemical, and isotopic relationships. *Econ. Geol.* **79**, 1703-1726.
- TAYLOR, R.G. (1979): *Geology of Tin Deposits*. Elsevier, Amsterdam, The Netherlands.
- VON GOERNE, G., FRANZ, G. & HEINRICH, W. (2001): Synthesis of tourmaline solid solutions in the system Na₂O–MgO–Al₂O₃–SiO₂–B₂O₃–H₂O–HCl and the distribution of Na between tourmaline and fluid at 300 to 700°C and 200MPa. *Contrib. Mineral. Petrol.* **141**, 160-173.
- WEISS, D. (1969): Bestimmung von Eisen(II)-oxid in Tourmalinen. *Chemische Zvesti* **23**, 671-676.
- WILLIAMSON, B.J., SPRATT, J., ADAMS, J.T., TINDLE, A.G. & STANLEY, C.J. (2000): Geochemical constraints from zoned

- hydrothermal tourmalines on fluid evolution and tin mineralization: an example from fault breccias at Roche, SW England. *J. Petrol.* **41**, 1439-1453.
- WOOD, S.A. & SAMSON, I. (1998): Solubility of ore minerals and complexation of ore metals in hydrothermal solutions. *In Techniques in Hydrothermal Ore Deposits Geology* (J.P. Richards & P.B. Larson, eds.). *Rev. Econ. Geol.* **10**, 33-80.
- YU, J.-M. & JIANG, S.-Y. (2003): Chemical composition of tourmaline from the Yunlong tin deposit, Yunnan, China: implications for ore genesis and mineral exploration. *Mineral. Petrol.* **77**, 67-84.
- Received June 22, 2005, revised manuscript accepted March 23, 2006.*